Steady-state light-induced forces for atom lithography

A. V. Bezverbny
Maritime State University, Vladivostok 690059, Russia

O. N. Prudnikov and A. V. Taichenachev
Novosibirsk State University, Pirogova 2, Novosibirsk 630090, Russia

A. M. Tumaikin and V. I. Yudin
Institute of Laser Physics SB RAS, Lavrentyeva 13/3, Novosibirsk 630090, Russia
(Received 27 August 2004; published 4 August 2005)

The light-induced force on an atom is calculated for an arbitrary field configuration, taking into account the spontaneous emission and optical pumping processes as well as the degeneracy of atomic energy levels. Two types of the optical transitions are analyzed: $J \to J$ with J a half-integer and $J \to J+1$ with J an arbitrary. Though the force is not potential in the general case, we introduce a scalar function Ψ, which plays a role of the potential energy, determining regions of localization of atoms. Applications of these results to atom nanolithography are discussed.

DOI: 10.1103/PhysRevA.72.023404 PACS number(s): 32.80.Lg, 32.80.Pj

I. INTRODUCTION

Atom lithography with a direct deposition (DD) technique is one of the useful applications of the light-induced forces for the production of nanostructures. Here a planar configuration of polarized light beams, acting like a mask on a previously collimated atomic beam, generates thickness-modulated structures on a suitable substrate (Fig. 1). Current results and potential applications of atomic nonofabrication are subjects of topic reviews [1,2]. The first successful DD results [3] with chromium atoms in a one-dimensional (1D) standing light wave have shown that both the high spatial resolution (better than 20 nm) and effective use of the nanostructures are possible. Then the field configurations with two and three noncollinear monochromatic light beams were used for the formation of 2D atomic periodic spatial structures [4,5]. It was shown that the spatial gradients of the light intensity [3–5] as well as the light polarization [6] can be used for the generation of a suitable optical potential.

Two different regimes of the light masks have been considered so far. In the first case (see, e.g., [1,2]), it is assumed that atoms interact with a far off resonance light field in a coherent manner. The effect consists of the focusing of an atomic beam in conservative adiabatic potentials, originating from the spatially modulated energy light shifts. The influence of the spontaneous emission on the focusing is considered to be negligible owing to large light detunings and short interaction times. This regime can be easily implemented experimentally, using high power lasers. The other dissipative regime for the light masks has been presented recently in [7,8]. It combines the focusing with the laser cooling (i.e., with the collimation of an atomic beam), resulting, at least in principle, in smaller width and in higher contrast of spatial atomic structures. In the framework of this method there are conservative (optical potential), dissipative (friction), and random (diffusion) contributions to the total light force on an atom. Note that the problem on cooling and localization of atoms in a standing wave has been thoroughly considered by Kazantsev and co-workers [9], using a simple atomic model with two nondegenerate levels.

In the present paper we consider the influence of the spontaneous emission and optical pumping on the spatial structure of the light force on an atom at rest $\mathbf{F}_0(\mathbf{r})$. We are motivated by the following. First, in the typical experimental conditions (see, e.g., [1,2]) the atom-light interaction time (100 ns) exceeds the excited-state relaxation time (10 ns), and, consequently, one cannot completely neglect the spontaneous relaxation and optical pumping processes. Second, in the regime of dissipative light mask [7,8], the force and its fluctuations should be calculated having regard to the optical pumping. As we will see, the incoherent part of the atom-light interaction can be significant, leading to changes in the

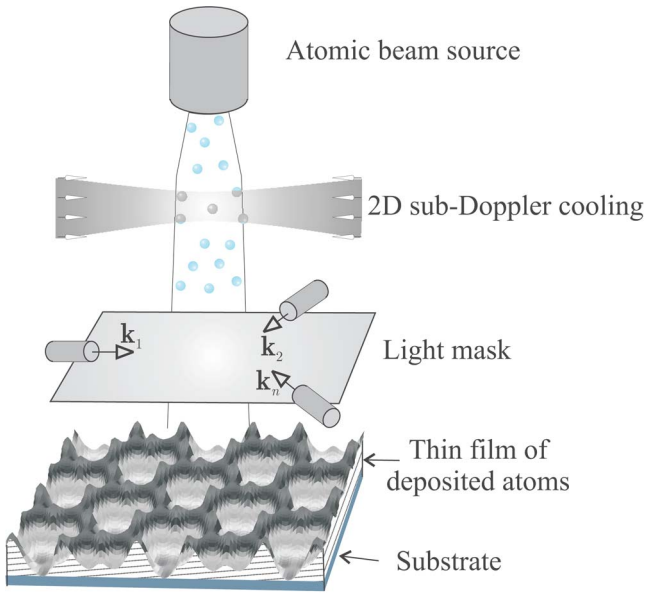

FIG. 1. (Color online) Basic scheme of atom lithography with direct deposition of atoms on substrate.

spatial structure of the optical potential. In the steady-state regime, when the atom-light interaction time exceeds the optical pumping time, we obtain compact analytical expressions for $\mathbf{F}_0(\mathbf{r})$ in a monochromatic field of arbitrary spatial and polarization structure, and of arbitrary intensity. The spatial structure of $\mathbf{F}_0(\mathbf{r})$ and its dependence on the field invariants are studied in 1D as well as in 2D cases. These results can be applied to both the conservative and dissipative light masks. In particular, we show that the optical pumping in a $lin \perp lin$ light configuration leads to a significant reduction of spherical aberrations in the case of $J \rightarrow J+1$ atomic transitions with large J. Using a semiclassical method based on the stochastic Newton equations (Langevin equation), we numerically simulate the focusing for several 1D and 2D light configurations. Both subwavelength structures and high contrast are observed in the atomic spatial distribution.

II. STATEMENT OF THE PROBLEM

We consider a beam of atoms with the total angular momenta J_g in the ground state and J_e in the excited state. The atomic transition $J_g \rightarrow J_e$ is resonantly driven by a monochromatic field formed by s coherent polarized light beams with wave vectors $\mathbf{k}_n$, lying in the plane orthogonal to the atomic beam direction:

$$\mathbf{E}(\mathbf{r},t) = e^{-i\omega t}\mathbf{E}(\mathbf{r}) + \text{c.c.},$$

$$\mathbf{E}(\mathbf{r}) = \sum_{n=1}^{s} e^{i\mathbf{k}_n\cdot\mathbf{r}}\mathbf{E}_n = e^{i\Phi}\mathcal{E}\mathbf{e}, \tag{1}$$

where the unit polarization vector $\mathbf{e}$ $[(\mathbf{e}^*\cdot\mathbf{e})=1$ and $\mathrm{Im}(\mathbf{e}\cdot\mathbf{e})=0]$, the phase Φ, and the real amplitude $\mathcal{E}$ of the total field are functions of the spatial coordinates $\mathbf{r}$. Hereinafter we shall use the following scalar field invariants $\mathcal{E}^2=\mathbf{E}\cdot\mathbf{E}^*$ and $\mathcal{I}=\mathbf{E}\cdot\mathbf{E}=e^{2i\Phi}(\mathbf{e}\cdot\mathbf{e})\mathcal{E}^2$. The first invariant $\mathcal{E}^2$ is proportional to the local energy density (intensity), and the other invariant $\mathcal{I}$ contains information on the local phase and polarization of the field. In particular, the degree of linear polarization can be expressed as $\ell=(\mathbf{e}\cdot\mathbf{e})=\sqrt{\mathcal{I}\cdot\mathcal{I}^*}/\mathcal{E}^2$.

In general, the atomic dynamics in a resonant light field is described by the quantum kinetic equations for the density matrix, taking into account the exchange of the energy, linear momentum, and angular momentum between atom and field. The linear momentum exchange gives rise to recoil of the atom, which is the basis of the mechanical action of light. The recoil effect is usually small, due to the smallness of the photon momentum ($\hbar k$) as compared to typical values of the atom momentum dispersion (Δp). This smallness leads to the two substantially different time scales in the evolution of an atomic ensemble [10,11]. The shorter one is connected with the optical pumping process and with ordering on the internal degrees of freedom. For atoms with a degenerate ground state the corresponding rate (reciprocal optical pumping time) can be estimated as $\Gamma_{\mathrm{op}}=\gamma\pi_e$, where γ is the excited-state radiative relaxation rate, and π_e is the total excited-state population (the probability that an atom is excited). The dynamics of the atomic distribution on the translational degrees of freedom is much slower. The corresponding rate is of the order of $(\hbar k/\Delta p)\Gamma_{\mathrm{scatt}}$, where Γ_{scatt} is the rate of scattering (spontaneous or stimulated) of photons by atom. As is well-known [10,11], at these conditions one can apply an approximate semiclassical treatment to the translational degrees of freedom. In such a way the classical notion of the light-induced force on atom emerges. In order to calculate the mean light force one has to find the atomic density matrix in the zeroth order in the photon recoil, i.e., one needs a solution of the generalized optical Bloch equations. In the general case of atom moving with arbitrary velocity in a spatially nonuniform field such a solution cannot be found analytically. However, for atomic beam precooled in the transverse directions down to the Doppler or sub-Doppler temperatures we can use the slow atom approximation [10], which is valid when the atom displacement during the optical pumping time is much less than the field spatial period $v(\Gamma_{\mathrm{op}})^{-1} \ll \lambda$. In this approximation the light force is expanded in series

$$\mathbf{F}(\mathbf{r},\mathbf{v}) = \mathbf{F}_0(\mathbf{r}) + \hat{\mathcal{X}}(\mathbf{r})\cdot\mathbf{v} + \cdots, \tag{2}$$

where $\mathbf{F}_0(\mathbf{r})$ is the force acting on atom at rest in $\mathbf{r}$. It is responsible for the focusing and localization of atoms. The symmetric part of the Cartesian tensor $\hat{\mathcal{X}}$ governs the process of linear momentum dissipation (friction). It should be noted that both $\mathbf{F}_0$ and $\hat{\mathcal{X}}$ can be decomposed in the field spatial gradients [11]:

$$\mathbf{F}_0 = \hbar\gamma\sum_{i=1}^{4} F_i\mathbf{g}_i,$$

$$\hat{\mathcal{X}} = \hbar\left[\sum_{i,j=1}^{4} X_{ij}\mathbf{g}_i\otimes\mathbf{g}_j + \sum_{l,m=5}^{6} X_{lm}\mathbf{g}_l\otimes\mathbf{g}_m\right]. \tag{3}$$

where $\mathbf{g}_i\otimes\mathbf{g}_j$ denotes the direct product of vectors $\mathbf{g}_i$ and $\mathbf{g}_j$. Here the field gradients $\mathbf{g}_n$ are defined by expressions

$$\mathbf{g}_1 = \boldsymbol{\nabla}\ln\mathcal{E}; \quad \mathbf{g}_2 = \boldsymbol{\nabla}\Phi; \quad \mathbf{g}_3 = \boldsymbol{\nabla}\ell;$$

$$\mathbf{g}_4 = \boldsymbol{\nabla}\phi; \quad \mathbf{g}_5 = \boldsymbol{\nabla}\alpha; \quad \mathbf{g}_6 = \boldsymbol{\nabla}\beta. \tag{4}$$

As is seen $\mathbf{g}_1$ is related to the intensity gradient, $\mathbf{g}_2$ is the gradient of the total phase, $\mathbf{g}_3$ is connected with the gradient of the ellipticity, and $\mathbf{g}_4$, $\mathbf{g}_5$, and $\mathbf{g}_6$ are gradients of three angles determining the orientation of the polarization ellipse with respect to the given coordinate frame. In particular, ϕ is the angle of the polarization ellipse orientation with respect to the axis orthogonal to the ellipse. The general properties of these $\mathbf{g}$-vectors in the vicinities of points with circular and linear polarizations, and near extremums of the intensity have been analyzed in [12].

In order to obtain analytical expressions for the coefficients F_i we need the atomic density matrix in the zeroth order both in the photon recoil and atomic velocity. It can be found in various approximations. Here we consider the steady-state regime, when the atom-light interaction time τ is much larger than the optical pumping time:

$$\Gamma_{\mathrm{op}}\tau \gg 1. \tag{5}$$

The corresponding steady-state density matrix has been found in the compact analytical form for all closed atomic transitions $J_g \to J_e$ [13]. These results are used in the following section to deduce analytical formulas for F_i.

III. LIGHT FORCE ON ATOM AT REST

As has been shown in [13] for the two types of optical transitions $J \to J-1$ and $J \to J$ with J an integer the steady-state optical coherence vanishes due to the coherent population trapping effect. Therefore for these transitions the steady-state light force on atom at rest is equal to zero. For the other two types $J \to J+1$ and $J \to J$ with J a half-integer the coefficients F_i are written as

$$F_1 = -2\tilde{\delta}\pi_e, \quad F_2 = \pi_e, \quad F_3 = -\frac{\tilde{\delta}\pi_e(1-A/\alpha_1)}{\ell},$$

$$F_4 = -\pi_e(A/\alpha_1)\sqrt{1-\ell^2}, \quad \pi_e = \frac{S\alpha_1}{\alpha_0 + 2S\alpha_1}, \tag{6}$$

where π_e is the total excited-state population, $\tilde{\delta} = \delta/\gamma$ is the detuning in γ units, and $S = 1/(2+8\tilde{\delta}^2)(I/I_{\mathrm{sat}})$ is the local saturation parameter defined in such a way that it is equal to $1/2$ at zero detuning and the intensity I equal to the saturation intensity $I_{\mathrm{sat}} = 2\pi^2\hbar\gamma c/(3\lambda^3)$ [14]. The other coefficients α_0, α_1, and A depend on the local field ellipticity only. The use of the results of the paper [15] leads to the following explicit expressions. In the case of $J \to J+1$ transitions:

$$\alpha_0 = \frac{1}{(2J+1)(4J+1)!\ell} \sum_{\substack{l=\kappa, \\ \kappa+2,\ldots}}^{2J} C_l P_l(\ell^{-1}),$$

$$\alpha_1 = P_{2J+1}(\ell^{-1}), \quad A = \frac{P'_{2J+1}(\ell^{-1})}{(2J+1)\ell},$$

$$C_l = (2l+1)(2J-l)!(2J+l+1)!,$$

where $P_n(x)$ are Legendre polynomials, $P'_n(x)$ are their derivative, $\kappa = 0$ for integer J, and $\kappa = 1$ for half-integer J. For the other type of $J \to J$ (J is a half-integer) transitions they read

$$\alpha_0 = \frac{4J(J+1)}{\ell} \sum_{l=1,3,\ldots}^{2J} C_l P_l(\ell^{-1}),$$

$$\alpha_1 = 2J+1, \quad A = 0,$$

$$C_l = (2l+1)\left[\frac{(l-1)!!}{l!!}\right]^2 \frac{(2J+l)!!}{(2J-l)!!}\frac{(2J-l-1)!!}{(2J+l+1)!!}.$$

The force $\mathbf{F}_0$ is a sum of the scattering (or radiation pressure) force

$$\mathbf{F}_{\mathrm{scatt}} = \hbar\gamma(F_2\mathbf{g}_2 + F_4\mathbf{g}_4)$$

and the dipole (or gradient) force

$$\mathbf{F}_{\mathrm{dip}} = \hbar\gamma(F_1\mathbf{g}_1 + F_3\mathbf{g}_3).$$

The scattering force is originated from the stimulated absorption and subsequent spontaneous emission of photons. It has absorptionlike even dependence on the detuning. The dipole force is caused by the coherent rescattering of photons between different laser beams. Since it has dispersive odd dependence on the detuning, its contribution into the force $\mathbf{F}_0$ dominates at large detunings $|\tilde{\delta}| \geqslant 10$. Thus the dipole force is of main interest for atom lithography applications. However, various possible effects of the scattering force are also discussed below.

IV. DIPOLE FORCE

The results of the previous section [Eq. (6)] allow us to present the dipole force in the form of product of the total excited-state population $\pi_e(\mathbf{r})$ and the gradient of the dimensionless scalar function $\Psi(\mathbf{r})$:

$$\mathbf{F}_{\mathrm{dip}} = -\hbar\delta\pi_e(\mathbf{r})\nabla\Psi(\mathbf{r}). \tag{7}$$

In the general case, the dipole force is not potential. Nevertheless, the function Ψ plays a role of the potential energy in many aspects. For example, all equilibrium points, where the dipole force vanishes, correspond to minima or maxima of Ψ. Zeros of the total excited-state population $\pi_e(\mathbf{r})$ do not give additional equilibrium points, as it is seen from the explicit expressions for Ψ [Eqs. (8) and (10) below]. Moreover, at positive (negative) detuning the dipole force attracts atoms to the minima (maxima) of the function Ψ. Eventually, in the high-saturation limit, when $S\alpha_1/\alpha_0 \gg 1$, $\pi_e \approx 1/2$, the dipole force becomes potential with the potential proportional to Ψ.

A. Transitions $J \to J$ with J a half-integer

For these transitions the function $\Psi(\mathbf{r})$ has the form

$$\Psi = \ln(|\mathcal{I}|). \tag{8}$$

The dipole force $\mathbf{F}_{\mathrm{dip}}$ is not saturated at high intensities in the vicinity of points with circular polarization ($\ell = 0$). Here it can be approximated as $\mathbf{F}_{\mathrm{dip}} \approx -\nabla U$ in terms of the effective potential [16]:

$$U_{\mathrm{eff},1} = \hbar\delta S \frac{1}{(2J)(2J+2)}\left[\frac{(2J)!!}{(2J-1)!!}\right]^2 \ell^{2J+1}. \tag{9}$$

The absence of the saturation in the case of pure circular polarization (say σ_+) of the total field is physically obvious because all atoms are optically pumped into the dark state $|J_g, m_g = J_g\rangle$. Correspondingly, in these points the light-induced force $\mathbf{F}_0$ vanishes and the potential $U_{\mathrm{eff},1}$ has minimum at positive detunings for arbitrary field configurations.

When $\ell \neq 0$ the dipole force $\mathbf{F}_{\mathrm{dip}}$ has the following properties. In the high-saturation limit $S\alpha_1/\alpha_0 \gg 1$ it is completely determined by the optical potential

$$U_{\mathrm{eff},2} = \frac{\hbar\delta}{2}\ln(|\mathcal{I}|).$$

At moderate saturation $S \lesssim 1$ the force is not purely potential. It can be seen that the equilibrium points, where $\mathbf{F}_{\mathrm{dip}} = \mathbf{0}$, are

governed by the extremums of the function $|\mathcal{I}|=|\mathbf{E}\cdot\mathbf{E}|$ rather than by the spatial distribution of the light intensity. Moreover, the nodes of the total field ($\mathbf{E}=\mathbf{0}$) are the localization points at positive detunings. Therefore there exists the regime of atom lithography with $\delta>0$, when atoms are attracted to the points of circular polarization and to the field nodes in arbitrary light mask. Additional localization points can arise from the local minima of the function $|\mathcal{I}|$. For negative detunings the atomic spatial distribution is exclusively determined by the maxima of the function $|\mathcal{I}|$. In the general case, their positions do not coincide with the points of pure linear polarization and the local maxima of the intensity. Although such a coincidence takes place for commonly used symmetrical light field configurations [12].

B. Transitions $J\rightarrow J+1$

Here the scalar function Ψ in Eq. (7) is given by

$$\Psi=\frac{1}{2J+1}\ln[(\mathcal{E}^2\ell)^{2J+1}P_{2J+1}(\ell^{-1})], \tag{10}$$

where the function $\ell^{2J+1}P_{2J+1}(\ell^{-1})$ is even in ℓ. It is maximal at circular polarization ($\ell=0$) and it monotonically decreases as the degree of linear polarization increases $|\ell|\rightarrow 1$. In the high-saturation limit the force $\mathbf{F}_{\mathrm{dip}}$ corresponds to the potential

$$U_{\mathrm{eff},3}=\frac{\hbar\delta}{2}\Psi.$$

In the general case the dipole force contains a vortical component in addition to the potential one. However, the effect of the vortical component on the spatial position of the localization points is negligibly small.

For this type of transition the localization points are determined by the spatial distributions both of the light intensity and of the second invariant function $|\mathcal{I}|$. In the general case, these points do not coincide either with points of circular (linear) polarization or with nodes (antinodes) of the field. In other words, they are governed by the spatial structures of the three functions $\mathcal{E}(\mathbf{r})$, $\ell(\mathbf{r})$, and $\Psi(\mathbf{r})$, simultaneously.

V. SCATTERING FORCE

The scattering force $\mathbf{F}_{\mathrm{scatt}}$ in light masks plays an important role in spite of its smallness (as $\gamma/|\delta|$) with respect to the dipole force $\mathbf{F}_{\mathrm{dip}}$ at large detunings because the spatial structures of these two forces are fundamentally different for multidimensional light field configurations. For example, the scattering force always vanishes in points where the polarization is circular. It has vortical structure $\mathbf{C}\times\delta\mathbf{r}$ in the vicinity of these points ($\delta\mathbf{r}\rightarrow 0$), where $\mathbf{C}$ is a constant vector [12]. Below we discuss other properties of the scattering force for the two types of transitions separately.

A. Transitions $J\rightarrow J$ with J a half-integer

Here the scattering force has the form

$$\mathbf{F}_{\mathrm{scatt}}=\frac{\hbar\gamma\pi_e\mathbf{H}}{4(2J+1)\mathcal{E}^4\ell^2};\quad \mathbf{H}=i(\mathcal{I}\nabla\mathcal{I}^*-\mathcal{I}^*\nabla\mathcal{I}). \tag{11}$$

Let us consider the vicinity $\mathbf{r}$ of an arbitrary point $\mathbf{r}_0$ and expand the function $\mathcal{I}$ up to the second order in small variation $\delta\mathbf{r}=\mathbf{r}-\mathbf{r}_0$

$$\mathcal{I}\approx\mathcal{I}_0+\mathbf{C}\cdot\delta\mathbf{r}+\delta\mathbf{r}\cdot\hat{\mathcal{D}}\cdot\delta\mathbf{r},$$

where $\mathcal{I}_0=\mathcal{I}(\mathbf{r}_0)$, and $\hat{\mathcal{D}}$ is a symmetrical tensor. Then, we have

$$\mathbf{H}=2\,\mathrm{Im}(\mathcal{I}_0\mathbf{C}^*+2\mathcal{I}_0\hat{\mathcal{D}}^*\cdot\delta\mathbf{r})+i\delta\mathbf{r}\times[\mathbf{C}\times\mathbf{C}^*].$$

The first term has a potential origin, whereas the second one is a vortical vector. The distinction between potential components of the scattering force $\mathbf{F}_{\mathrm{scatt}}^{\mathrm{pot}}$ and of the dipole force $\mathbf{F}_{\mathrm{dip}}^{\mathrm{pot}}$ consists of the different net effects under spatial averaging over some trajectory of length l: $\langle\mathbf{F}\rangle_l=l^{-1}\int\mathbf{F}d\mathbf{l}$. Usually, the average dipole force $\langle\mathbf{F}_{\mathrm{dip}}\rangle_l$ vanishes for periodical or quasiperiodical symmetrical field configurations, when $l\gg\lambda$. The exception is the dipole force rectification ($\langle\mathbf{F}_{\mathrm{dip}}\rangle_l\neq 0$) in some specific field configurations (1D examples have been discussed in [15]). By contrast, the average scattering force increases with l as a rule, for instance, due to the intensity imbalance of light beams (a simple 1D example is a plane running wave). Its influence leads to a directed drift of atoms. The vortical component of the scattering force can also lead to directed flows of atoms on large spatial scales $l\gg\lambda$.

B. Transitions $J\rightarrow J+1$

For these transitions the scattering force is given by

$$\mathbf{F}_{\mathrm{scatt}}=-\frac{\hbar\gamma\pi_e}{\alpha_1\mathcal{E}^2}\left(A\mathbf{G}+\frac{P'_{2J}(\ell^{-1})\mathbf{H}}{4(2J+1)(\mathcal{E}\ell)^2}\right),$$

$$(\mathbf{G})_i=\mathrm{Im}\sum_j(\mathbf{E})_j\nabla_i(\mathbf{E}^*)_j. \tag{12}$$

Here the vector $\mathbf{G}$ is vortical: $\boldsymbol{\nabla}\cdot\mathbf{G}=0$. Thus we have basically an additional contribution to the vortex component of the light force. This contribution becomes essential in the vicinity of points with circular field polarization.

VI. 1D FIELD CONFIGURATIONS

In this section we consider symmetrical one-dimensional field configurations, where the light force corresponds to a periodic potential, which are most interesting in the context of atom lithography. All such configurations are formed by two counterpropagating (along the z axis) light waves with equal amplitudes E_s. They can be unambiguously classified by three parameters: the angle θ between the major semiaxes of the polarization ellipses of the waves, and two ellipticity angles ε_1 and ε_2. The ellipticity angle is defined in such a way that $|\tan\varepsilon|$ is equal to the ratio of the minor ellipse axis to the major one, and the sign of ε governs the helicity. Thus in this section we consider $\varepsilon_1-\theta-\varepsilon_2$ field configurations at some specific values of the parameters. As we will see, a

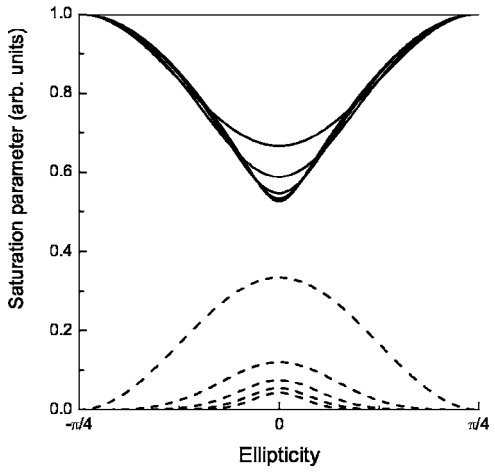

FIG. 2. The effective saturation parameter (arbitrary units) vs the ellipticity angle in an elliptically polarized standing wave. Solid lines correspond to $J \rightarrow J+1$ transitions; J runs from 0 to 4 (from top to bottom). Dashed lines correspond to $J \rightarrow J$ transitions $J = 1/2, 3/2, \ldots, 9/2$ (from top to bottom).

variety of 1D potentials can be generated depending on the polarization of light waves and on the type of atomic transition. We have always two simple rules. First, all equilibrium points, where the dipole force vanishes, correspond either to maxima or minima of the function Ψ. Second, at large $\delta > 0 (\delta < 0)$ atoms are attracted to minima (maxima) of the function Ψ.

A. Simple 1D configurations

Let us start with two simple 1D field configurations, used as elementary examples, where just one from four gradients $\mathbf{g}_i$ is not equal to zero.

1. Standing wave with elliptical polarization

In this case the phase and polarization of the total field do not depend on the coordinate, and $S(z) = 2S_0[1 + \cos(2kz)]$, where S_0 is the saturation parameter per single beam. The force has the form

$$F(z) = -\frac{\partial}{\partial z} U(z);$$

$$U(z) = \frac{\hbar \delta}{2} \ln\left[1 + \frac{2\alpha_1}{\alpha_0} S(z)\right]. \tag{13}$$

As is seen, the analytical expression for the optical potential is similar to that for a two-level atom with nondegenerate levels [9]. However, the effective saturation parameter $S_{\text{eff}} = S\alpha_1/\alpha_0$ depends now on the transition type and on the light polarization (see Fig. 2). The focusing properties of a standing wave are well known. At positive (negative) detuning atoms are attracted to field nodes (antinodes).

2. The lin ⊥ lin field configuration

The well-known *lin* ⊥ *lin* light field configuration is a superposition of two counterpropagating plane waves with orthogonal linear polarizations. In this case the gradients of the phase and intensity vanish, the polarization ellipse orientation is constant, and the ellipticity changes according to the relationship $\ell = \cos(2kz)$. The dipole force can be written as

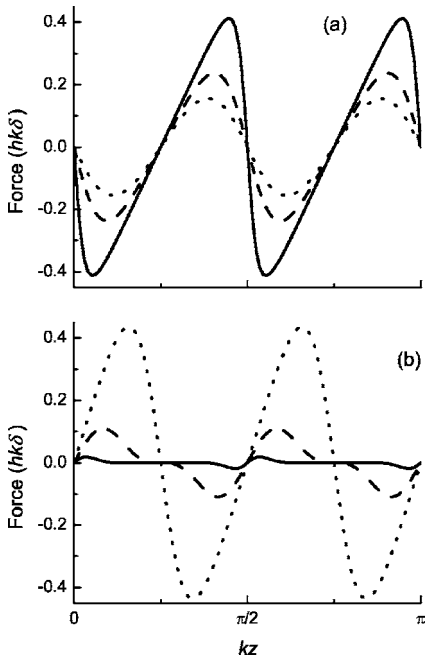

FIG. 3. The dipole force in $\hbar k \delta$ units vs kz in the *lin* ⊥ *lin* configuration. (a) $J \rightarrow J+1$ transitions with $J = 1/2$ (dotted line), $J = 1$ (dashed line), and $J = 4$ (solid line). (b) $J \rightarrow J$ transitions with $J = 1/2$ (dotted line), $J = 3/2$ (dashed line), and $J = 9/2$ (solid line). The single-beam saturation parameter $S_0 = 1$.

$$F(z) = -\frac{\partial}{\partial z} U(\cos(2kz));$$

$$U(\ell) = \hbar \delta \int \frac{\pi_e (1 - A/\alpha_1)}{\ell} d\ell. \tag{14}$$

The results of calculations by the formula (14) are shown in Fig. 3 for several atomic transitions. As is seen, the coordinate dependence of the force is qualitatively different for the two types of transitions. First of all, the force has opposite signs for $J \rightarrow J+1$ and for $J \rightarrow J$ (J is a half-integer) transitions. Then, in the case of the transitions $J \rightarrow J$ (J is a half-integer) in the vicinity of equilibrium points with circular polarizations, where $\ell = \cos(2\varepsilon) \rightarrow 0$, the force is anharmonic, except for the case $J = 1/2$. Indeed, according to Eq. (9), the force varies as ℓ^{2J}. For the transitions $J \rightarrow J+1$ we observe the opposite behavior. As the angular momentum J increases the shape of the force spatial dependence approaches triangular, i.e., the length of areas (around the points with $\ell = 0$) of the linear (harmonic) dependence increases. This effect is more profound in the high-saturation regime $S \gg 1$, when $\pi_e \approx 1/2$, and the potential can be approximated as

$$U(\ell) \approx \frac{\hbar\delta}{2(2J+1)} \ln[\ell^{2J+1} P_{2J+1}(\ell^{-1})].$$

One can expect a significant reduction of the spherical aberrations for the $J \rightarrow J+1$ transitions with large J, when atoms are focused into the points with circular polarizations at $\delta < 0$, in comparison with the case of small J or with the optical potential in a standing wave. The other difference between the two types of transitions manifests in the potential depth at $S \gg 1$. For the case of $J \rightarrow J+1$ transitions the depth is saturated and does not exceed $\hbar\delta \ln(2)/2$, while for the $J \rightarrow J$ case it scales as $\ln(S)$ (for instance, the depth is equal to $\hbar\delta \ln(1+3S/2)/4$ in the case of $1/2 \rightarrow 1/2$ transition).

B. 1D field configurations formed by elliptically polarized waves

Proceed with more complicated field configurations, where two and four gradients $\mathbf{g}_i$ differ from zero simultaneously. Among all $\varepsilon_1 - \theta - \varepsilon_2$ field configurations we can distinguish three symmetrical classes, for which the optical potential is periodic or, alternatively, the light force on an atom at rest vanishes under spatial averaging over the field period λ. The first of these classes corresponds to $\varepsilon_1 = -\varepsilon_2 = \varepsilon$ and it will be referred to as $\varepsilon - \theta - \bar{\varepsilon}$. The second one $\varepsilon \perp \varepsilon$ is a one-parametric class, where $\varepsilon_1 = \varepsilon_2 = \varepsilon$ and $\theta = \pi/2$. The third class consists of elliptically polarized standing waves ($\varepsilon_1 = \varepsilon_2 = \varepsilon$ and $\theta = 0$) and it is already considered above.

1. The $\varepsilon \perp \varepsilon$ field configuration

In this case the scalar field invariants take the form

$$\mathcal{E}^2 = 2E_s^2[1 - \sin(2\varepsilon)\sin(2kz)],$$

$$\mathcal{I} = 2E_s^2 \cos(2\varepsilon)\cos(2kz). \tag{15}$$

The gradients of the phase and of the angle ϕ vanish. Consequently, the scattering force is zero for this configuration. If $\varepsilon \neq 0$, both the intensity and ellipticity are spatially nonuniform. Equation (15) shows that extremal points of the intensity $I \sim \mathcal{E}^2$ are correlated with points of circular polarization, where $\ell = \cos(2\varepsilon)\cos(2kz)/[1 - \sin(2\varepsilon)\sin(2kz)] = 0$. In these points $2kz = \pi/2(2n+1)$ the function Ψ [see Eqs. (8) and (10)] is maximal in the case of $J \rightarrow J+1$ transitions, and it has minima at these points for the $J \rightarrow J$ transitions. The spatial dependence of the dipole force is shown in Fig. 4. One can observe double-well potential structures. These structures appear at positive detuning for the $J \rightarrow J+1$ transitions near the intensity minima. In the case of $J \rightarrow J$ transitions double potential wells appear at negative detuning around the intensity maxima.

2. The $\varepsilon - \theta - \bar{\varepsilon}$ field configuration

Here the field invariants read

$$\mathcal{E}^2 = 2E_s^2[1 + \cos\theta \cos(2\varepsilon)\cos(2kz)],$$

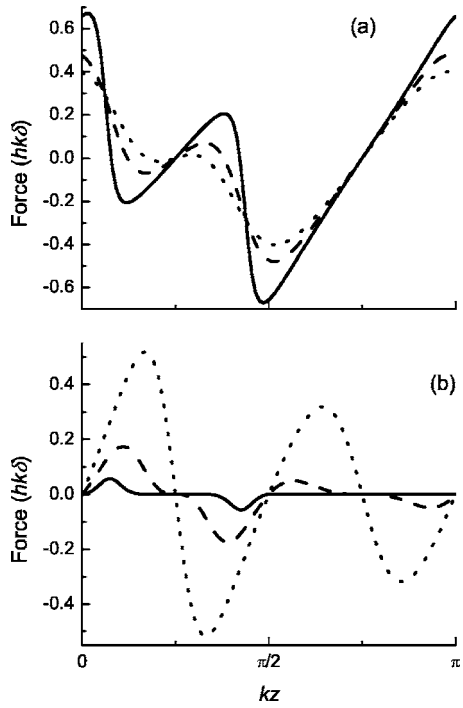

FIG. 4. The dipole force in $\hbar k\delta$ units vs kz in the $\varepsilon \perp \varepsilon$ configuration. (a) $J \rightarrow J+1$ transitions with $J = 1/2$ (dotted line), $J = 1$ (dashed line), and $J = 4$ (solid line). (b) $J \rightarrow J$ transitions with $J = 1/2$ (dotted line), $J = 3/2$ (dashed line), and $J = 9/2$ (solid line). The single-beam saturation parameter $S_0 = 1$, and the ellipticity angle $\varepsilon = \pi/16$.

$$\mathcal{I} = 4E_s^2[\cos\theta + \cos(2\varepsilon)\cos(2kz) + i\sin\theta \sin(2\varepsilon)], \tag{16}$$

and, generally speaking, all four gradients $\mathbf{g}_i$ (where $i = 1, \ldots, 4$) are not equal to zero. The intensity extremums correlate with points of the field linear polarization, where $\ell = 1$. In these points the function Ψ is maximal in the case of $J \rightarrow J$ transitions. For the $J \rightarrow J+1$ transitions in the intensity minima the function Ψ is also minimal. However, in the intensity maxima the function Ψ can be either minimal or maximal, depending on the angular momentum J and on the field parameters θ and ε. When the ellipticity angle is sufficiently small and the orientation angle is sufficiently close to $\pi/2$, double-well potential structures can appear (see Fig. 5). They are situated near the intensity maxima for the $J \rightarrow J+1$ transitions at $\delta < 0$, and near the intensity minima in the case of $J \rightarrow J$ transitions at $\delta > 0$. Since the phase and angle gradients differ from zero in the general case ($\varepsilon \neq 0$, $\pm\pi/4$ and $\theta \neq 0$), the scattering force contributes to the optical potential. The scattering force vanishes in the points of linear polarization. At small detunings $|\delta| \approx \gamma$ the scattering force deforms the optical potential substantially.

C. Numerical simulations

In this section we describe numerical simulations of the focusing in the *lin* ⊥ *lin* field configuration. The simulations are based on the semiclassical stochastic method introduced in the laser cooling theory by Javanainen [17]. As we wrote

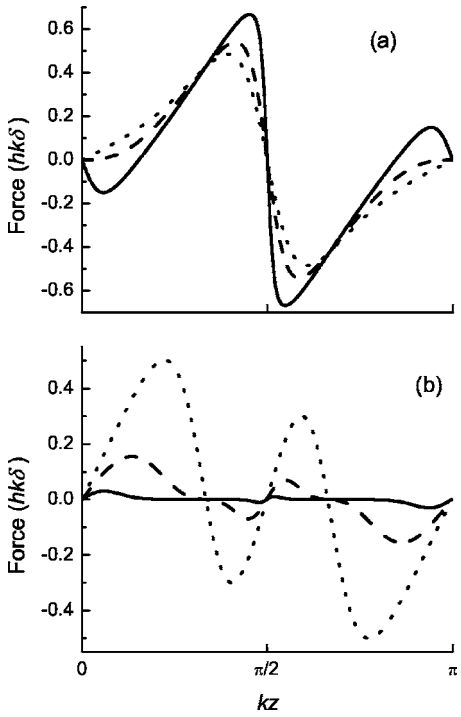

FIG. 5. The dipole force in $\hbar k\delta$ units vs kz in $\varepsilon-\theta-\bar{\varepsilon}$ configuration. (a) $J\rightarrow J+1$ transitions with $J=1/2$ (dotted line), $J=1$ (dashed line), and $J=4$ (solid line). (b) $J\rightarrow J$ transitions with $J=1/2$ (dotted line), $J=3/2$ (dashed line), and $J=9/2$ (solid line). The single-beam saturation parameter $S_0=1$, and the angles are $\theta=\pi/3$ and $\varepsilon=\pi/32$.

above, the dipole force F_0 on an atom at rest has approximately triangular spatial dependence for the $J\rightarrow J+1$ optical transitions at large J [see Fig. 3(a)]. Thus the area where the optical potential has the parabolic shape increases with J and we expect a significant reduction of the spherical aberrations.

Apart from the force $\mathbf{F}_0$ we take into cosideration the friction force (first order corrections in the atomic velocity) and the random component, corresponding to the momentum diffusion coefficient. It is worth noting that relative influences of the dissipative and random forces on the atomic spatial distribution, compared to the main focusing force $\mathbf{F}_0$, depend on the parameters of the problem (light detuning and intensity, interaction time, initial divergency of atomic beam, etc.), the light field configuration, and on the type of atomic transition. In many cases the dissipative and random contributions are negligible. Nevertheless, for the sake of the universality of numerical routines, we take into account both these factors.

We study focusing for two different atomic transitions $1/2\rightarrow 3/2$ and $4\rightarrow 5$. The other parameters correspond to the case of Cs atoms. In Fig. 6 the spatial dependencies of the optical potential $U(z)$, friction $\xi(z)$, and diffusion $D(z)$ coefficients are shown. Sharp features in $\xi(z)$ and $D(z)$ are seen in the case of large angular momenta $4\rightarrow 5$. Note that the friction and diffusion are small near the potential minima, where atoms are focused, this makes their effects on the spatial atomic distribution less significant.

In our simulations we assume that the initial atomic momentum distribution is Gaussian with the width $\Delta p_\perp=10\hbar k$.

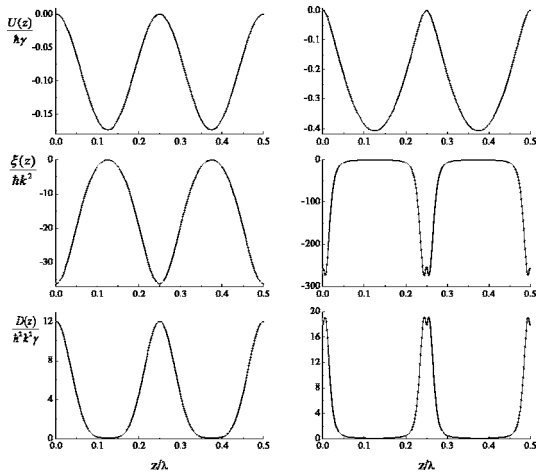

FIG. 6. Spatial dependences of the optical potential $U(z)$, friction $\xi(z)$, and diffusion $D(z)$ coefficients for atoms with $1/2\rightarrow 3/2$ (left panel) and $4\rightarrow 5$ (right panel) optical transition in the $lin\perp lin$ field configuration with the single-beam saturation parameter $S_0=0.158$ and detuning $\delta=-5\gamma$.

The spatial distribution of atoms are shown in Fig. 7. One can see narrow, subwavelength spatial structures [the FWHM widths are $\Delta z=0.051\lambda$ in Fig. 7(a) and $\Delta z=0.038\lambda$ in Fig. 7(b)] formed due to the focusing in the thick lens regime. The interaction time is equal to a quarter of the oscillation period in the potential $U(z)$ ($t_{int}=49.16\gamma^{-1}$ and $t_{int}=41.37\gamma^{-1}$ in the cases of $1/2\rightarrow 3/2$ transition and $4\rightarrow 5$ transition, respectively). The difference in the spot size Δz in these cases can be related to the differences in dissipative and random forces (see Fig. 6). As is seen from Fig. 7, the pedestal is significantly reduced in the case of $4\rightarrow 5$ transi-

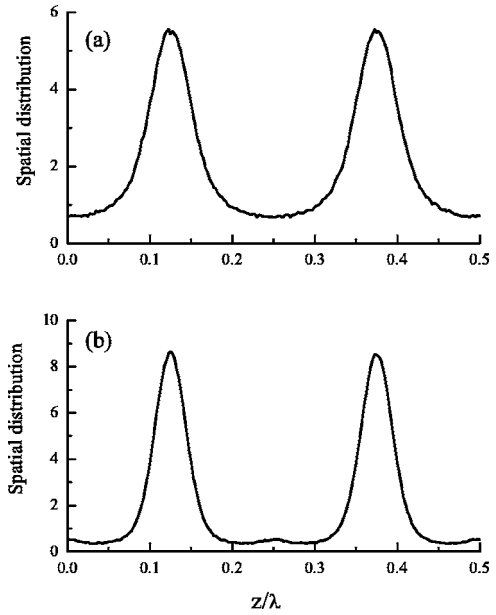

FIG. 7. The spatial distribution of focused atoms in the $lin\perp lin$ field configuration with the single-beam saturation parameter $S_0=0.158$ and detuning $\delta=-5\gamma$. (a) The case of $1/2\rightarrow 3/2$ transition and (b) the case of $4\rightarrow 5$ transition. The interaction time in both cases corresponds to a quarter of the oscillation period.

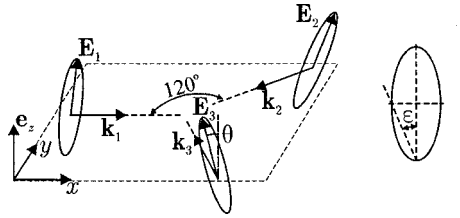

FIG. 8. Three-beam light configuration (left) and the polarization ellipse of a beam (right), where ε is the ellipticity angle.

tions (the ratio of the pedestal area to the total area $\mathcal{R}=0.19$) compared to the case of $1/2\rightarrow 3/2$ transition ($\mathcal{R}=0.35$). It confirms our expectations of the reduced spherical aberrations.

VII. 2D FIELD CONFIGURATIONS

We have examined some 2D field configurations, which are formed by three or four light beams. A wide range of correlations between spatial distributions of extremal points (minima and maxima) of the functions I, ℓ, and Ψ was observed. Thus in order to predict a possible spatial atomic distribution one has to analyze the interference patterns $I(\mathbf{r})$ and $\ell(\mathbf{r})$ for transitions $J\rightarrow J$ (J-half-integer) as well as the more complicated function $\Psi(\mathbf{r})$ for transitions $J\rightarrow J+1$. As an example we consider here the three-beam symmetrical configuration [12], where the light beams have identical ellipticity angles $\varepsilon_1=\varepsilon_2=\varepsilon_3=\varepsilon$ and amplitudes E_s (Fig. 8).

In this field configuration the field invariants read

$$\mathcal{E}^2 = E_s^2[3 + C(Z^*Z - 3)]; \quad Z = \sum_{n=1}^{3} e^{i\mathbf{k}_n\cdot\mathbf{r}};$$

$$\mathcal{I} = E_s^2[(1+2C)(Z^2 - 2Z^*) - 2D(Z^2 - 3Z^*)];$$

$$C = (\mathbf{e}_i\cdot\mathbf{e}_j^*)_{i\neq j}; \quad D = (\mathbf{e}_i\cdot\mathbf{e}_j)_{i\neq j},$$

where $\mathbf{e}_i=(\mathbf{e}_z+\boldsymbol{\epsilon}\cdot\mathbf{k}_i\times\mathbf{e}_z)/\sqrt{1+|\boldsymbol{\epsilon}|^2}$ is a polarization vector of the ith beam, the parameter $\boldsymbol{\epsilon}=(\tan\vartheta+i\tan\varepsilon)/(1-i\tan\vartheta\tan\varepsilon)$ is determined by the ellipticity angle ε and the orientation angle ϑ between the direction $\mathbf{e}_z$ perpendicular to the configuration plane and the longer axis of the beam polarization ellipse. One can see that under the condition $\tan^2\varepsilon_0=(3\cos 2\vartheta_0+1)/(3\cos 2\vartheta_0-1)$ the parameter C vanishes, and the total field intensity becomes spatially uniform. Consequently, when the configuration parameters are close to $\{\varepsilon_0,\vartheta_0\}$, the distributions $\Psi(\mathbf{r})$ and $I(\mathbf{r})$ are completely different and a strong correlation between $\Psi(\mathbf{r})$ and $\ell(\mathbf{r})$ is observed. An opposite situation of strong spatial correlations between I and Ψ takes place for the parameters $\varepsilon\rightarrow 0$, $\vartheta\rightarrow 0$. However, as a rule, in intermediate cases extremums of the functions I, ℓ, and Ψ do not coincide.

In Fig. 9 the spatial distributions of the intensity I (left), degree of linear polarization ℓ (center), and quasipotential function Ψ (right) are shown for an intermediate variant with parameters $\tan\varepsilon=2$, $\tan\vartheta=1/\sqrt{2}$. Here the Ψ-distribution is plotted for the transition $1\rightarrow 2$. It is worth noting that this

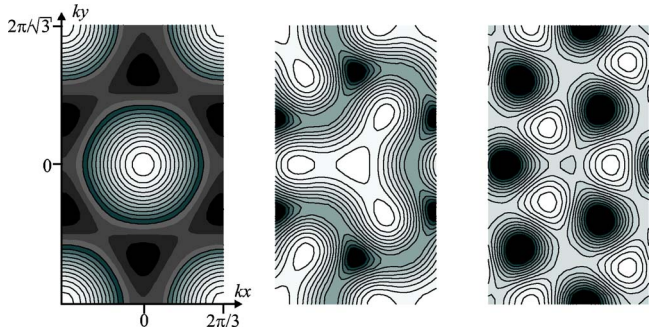

FIG. 9. (Color online) Grayscaled contour plots of the functions $I(\mathbf{r})$ (left), $\ell(\mathbf{r})$ (center), and $\Psi(\mathbf{r})$ (right). The bright (dark) regions show the maxima (minima) of these functions.

distribution has only a weak dependence on the angular momentum J. In Fig. 9 the spatial limits $|kx|\leqslant 2\pi/3$, $|ky|\leqslant 2\pi/\sqrt{3}$ correspond to the unit rectangular cell for this field configuration. It is seen from Fig. 9 that the maxima of the function Ψ are situated in intermediate positions between the extremums of I and ℓ, whereas the minima of Ψ correlate with the maxima of ℓ.

Numerical simulations

In this section we describe numerical simulations of the formation of periodic atomic distribution in the three-beam configuration. Here, much like the 1D case, the simulations are based on the semiclassical stochastic method [17]. Apart from the mean force $\mathbf{F}_0$ on an atom at rest we take into account the friction force $\mathbf{F}_{\rm diss}=\hat{\mathcal{X}}(\mathbf{r})\cdot\mathbf{v}$ and the random contribution $\mathbf{F}_{\rm rand}$ related to the momentum diffusion. We use the dimensionless Langevin equation

$$\frac{d\mathbf{P}}{d\tau} = \mathbf{f}_0 + \mathbf{f}_{\rm diss} + \mathbf{f}_{\rm rand}, \tag{17}$$

where the dimensionless time $\tau=t/t_{\rm trans}$, momentum $\mathbf{P}=\mathbf{p}/p_0$, and forces $\mathbf{f}=\mathbf{F}t_{\rm trans}/p_0$ are determined through the corresponding scales $p_0=\sqrt{\hbar\gamma m}$ and $t_{\rm trans}=1/\sqrt{2\omega_{\rm rec}\gamma}$. Here $\hbar\omega_{\rm rec}=(\hbar k)^2/(2m)$ is the recoil energy. The time scale is much greater than the excited-state relaxation time $t_{\rm trans}\gg 1/\gamma$ and it governs the evolution on the translational degrees of freedom.

In order to compare the spatial atomic distribution with the distributions of the field invariants we choose the same parameters as in Fig. 9, i.e., $\tan\varepsilon=2$, $\tan\vartheta=1/\sqrt{2}$, and transition $1\rightarrow 2$. It is assumed that the atomic beam has initially uniform spatial distribution within the unit cell. The other atomic parameters are the single-beam saturation parameter $S_0=0.25$; the detuning $\tilde{\delta}=-10$ or $\tilde{\delta}=10$; and the spread of the transverse velocities $\langle(\Delta v_\perp)^2\rangle=0.1\hbar\gamma/m$. The latter corresponds to the sub-Doppler precooling of the atomic beam. The average interaction time, the most important parameter of the numerical simulations, is determined by the ratio of

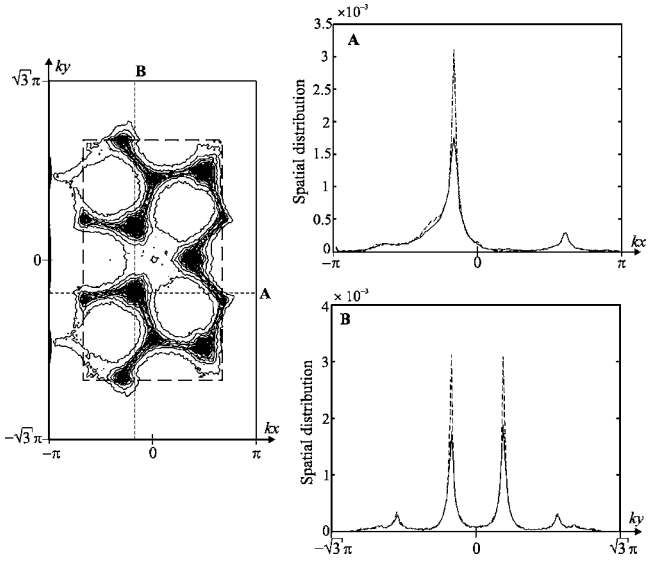

FIG. 10. The spatial atomic distribution in the three-beam light field configuration for the transition $1\rightarrow 2$, single-beam saturation parameter $S_0=0.25$, average interaction time $t_{\mathrm{int}}=0.6t_{\mathrm{trans}}$, and negative detuning $\delta=-10\gamma$. A contour plot is shown in the left panel, and the cross sections of the atomic distribution in two orthogonal directions **A** and **B** are shown in the right panel.

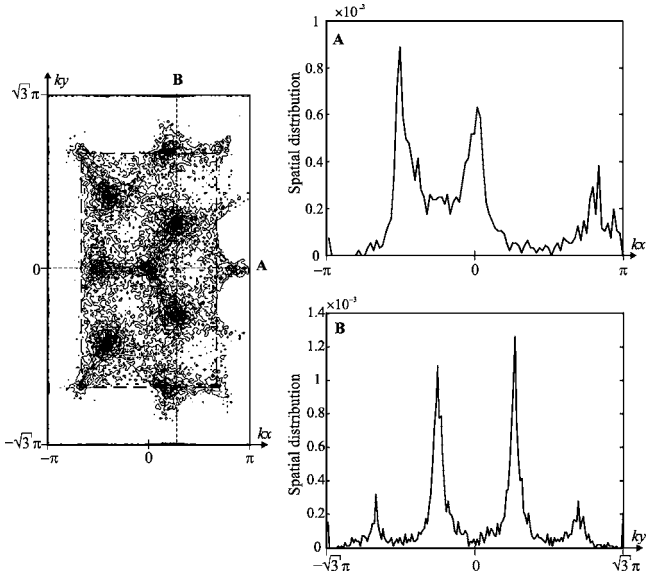

FIG. 11. The spatial atomic distribution in the three-beam light field configuration for the transition $1\rightarrow 2$, single-beam saturation parameter $S_0=0.25$, average interaction time $t_{\mathrm{int}}=0.6t_{\mathrm{trans}}$, and positive detuning $\delta=10\gamma$. A contour plot is shown in the left panel, and the cross sections of the atomic distribution in two orthogonal directions **A** and **B** are shown in the right panel.

the light beam diameter d_0 to the average longitudinal velocity $\langle v_z\rangle$: $t_{\mathrm{int}}=d_0/\langle v_z\rangle$. We also take into account the Maxwellian distribution on the longitudinal velocities v_z. We choose the average interaction time $t_{\mathrm{int}}=0.6t_{\mathrm{trans}}$. At this choice the effect of the force $\mathbf{F}_0$ on the atomic spatial distribution is crucial and appreciable. At the shorter interaction time the atomic spatial distribution remains practically unchanged. The opposite limit $t_{\mathrm{int}}\gg t_{\mathrm{trans}}$ corresponds to the dissipative optical lattice [18], where the (quasi)-stationary atomic distribution is governed by the three forces $\mathbf{F}_0$, $\mathbf{F}_{\mathrm{diss}}$, and $\mathbf{F}_{\mathrm{rand}}$ on an equal footing.

The results for the negative $\tilde{\delta}=-10$ and positive $\tilde{\delta}=10$ detuning are shown in Figs. 10 and 11, respectively. The spatial atomic distributions are plotted as contour plots in the extended rectangle with boundaries $|kx|\leqslant 1.5\times 2\pi/3$ and $|ky|\leqslant 1.5\times 2\pi/\sqrt{3}$. These distributions are the result of the light mechanical action on atoms, which are homogeneously distributed within the unit cell before the interaction. This cell is indicated in Figs. 10 and 11 as the dashed-line rectangle. The extended rectangle is split into 100×173 pieces, and the resulting atomic distributions are calculated by the count of atoms in each piece. The total number of atoms in the unit cell is chosen as 10^6 and 10^5 for Figs. 10 and 11, correspondingly. We also present in Figs. 10 and 11 the cross sections of the atomic distributions along certain orthogonal directions (**A**) and (**B**). The solid lines in these profiles show the normalized distributions calculated with allowance made for the dissipative and random forces, while the dashed lines in Fig. 10 correspond to the simulation without taking into account $\mathbf{f}_{\mathrm{diss}}$ and $\mathbf{f}_{\mathrm{rand}}$. One can see that the effect of dissipative and random forces on the spatial atomic distribution is not so significant in the case under consideration. The width of peaks and the pedestal are almost insensitive to $\mathbf{f}_{\mathrm{diss}}$ and $\mathbf{f}_{\mathrm{rand}}$. The influence of these forces manifests in the decrease of the peak maximum by a factor of about 2. By contrast, a role of the light-induced force $\mathbf{f}_0$ is crucial. Namely this force redistributes atoms into the maxima of Ψ for negative detunings $\tilde{\delta}<0$ (Fig. 10) or into the minima of Ψ for $\tilde{\delta}>0$ (Fig. 11).

In our calculations we vary $\tilde{\delta}$, S_0, t_{int}, and the individual beam parameters $E_{s,i}$, $\tilde{\varepsilon}_i$. We do not observe spatially ordered structures at small detunings $|\tilde{\delta}|<1$. This fact shows that the scattering force is not suitable for the purposes of atom lithography. However, in field configurations with broken symmetry, the scattering force as well as the rectified dipole force could push the atomic sample in certain preferred directions. The variations of S and $t_{\mathrm{int}}>0.5t_{\mathrm{trans}}$ do not lead to the appearance (or disappearance) of localization points, but they can significantly modify the degree of localization.

VIII. CONCLUSION

In this paper we have obtained and analyzed explicit expressions for the steady-state radiative force on an atom at rest $\mathbf{F}_0$. We have found the scalar function Ψ which plays a role of the potential, determining the localization points. All the results are valid for the closed (cycling) dipole transitions with arbitrary angular momenta J_g and J_e, and for a wide range of the light mask parameters (detuning δ, saturation S, light beam diameter d_0, etc.). The results are not restricted by 1D or 2D light configurations, and they can be useful in the case of 3D field configurations as well [19].

We have numerically simulated the focusing of the atomic beam for several 1D and 2D filed configurations, taking into account the dissipative force and momentum diffusion. In the

1D case we have pointed out the *lin* ⊥ *lin* field configuration. Here the optical potential for atoms with the dipole transitions $J \rightarrow J+1$ becomes harmonic almost everywhere at large J. In the nondissipative regime ($t \ll \omega_{rec}^{-1}$) a significant reduction of the spherical aberrations has been confirmed by the numerical simulations. We have studied a number of 2D field configurations for the longer interaction time ($t \simeq \omega_{rec}^{-1}$). The numerical simulations show that the spatial atomic distribution is governed by the main focusing force $\mathbf{F}_0$, while the dissipative $\mathbf{F}_{\mathrm{diss}}$ and random $\mathbf{F}_{\mathrm{rand}}$ forces modify the shapes of localization regions. Our results can be of experimental interest in the field of atom lithography.

ACKNOWLEDGMENTS

This work was partially supported by RFBR (Grants No. 04-02-16488 and No. 05-02-17086) and by a grant INTAS-01-0855. O.N.P. was supported by the grant for young scientists of the Novosibirsk Region Administration.

[1] M. K. Oberthaler and T. Pfau, J. Phys.: Condens. Matter **15**, R233 (2003).
[2] D. Meschede and H. Metcalf, J. Phys. D **36**, R17 (2003).
[3] J. J. McClelland, R. E. Scholten, E. C. Palm, and R. Celotta, Science **262**, 87 (1993).
[4] R. Gupta, J. J. McClelland, Z. J. Jabbour, and R. Celotta, Appl. Phys. Lett. **67**, 1378 (1995).
[5] U. Drodofsky, J. Stuhler, T. Schulze, M. Drewsen, B. Brezger, T. Pfau, and J. Mlynek, Appl. Phys. B: Lasers Opt. **65**, 755 (1997).
[6] B. Brezger, Th. Schulze, P. O. Schmidt, R. Mertens, T. Pfau, and J. Mlynek, Europhys. Lett. **46**, 148 (1999).
[7] R. Stutzle, D. Jurgens, A. Habenicht, and M. K. Oberthaler, J. Opt. B: Quantum Semiclassical Opt. **5**, S164 (2003).
[8] O. N. Prudnikov and E. Arimondo, J. Opt. B: Quantum Semiclassical Opt. **6**, 336 (2004).
[9] A. P. Kazantsev, G. I. Surdutovich, and V. P. Yakovlev, *Mechanical Action of Light on Atoms* (World Scientific, Singapore, 1990).
[10] A. P. Kazantsev, Usp. Fiz. Nauk **124**, 113 (1978) [Sov. Phys. Usp. **21**, 58 (1978)]; R. J. Cook, Phys. Rev. A **22**, 1078 (1980); V. G. Minogin, Zh. Eksp. Teor. Fiz. **79**, 2044 (1980) [Sov. Phys. JETP **52**, 1032 (1980)]; J. P. Gordon and A. Ashkin, Phys. Rev. A **21**, 1606 (1980); J. Dalibard and C. Cohen-Tannoudji, J. Phys. B **18**, 1661 (1985); J. Dalibard and C. Cohen-Tannoudji, J. Opt. Soc. Am. B **6**, 2023 (1989); Y. Castin and K. Mølmer, J. Phys. B **23**, 4101 (1990); G. Nienhuis, P. van der Straten, and S.-Q. Shang, Phys. Rev. A **44**, 462 (1991); J. Javanainen, *ibid.* **44**, 5857 (1991).
[11] A. V. Bezverbny, O. N. Prudnikov, A. V. Taichenachev, A. M. Tumaikin, and V. I. Yudin, Zh. Eksp. Teor. Fiz. **123**, 383 (2003) [J. Exp. Theor. Phys. **96**, 383 (2003)].
[12] A. V. Bezverbny, Zh. Eksp. Teor. Fiz. **124**, 875 (2003) [J. Exp. Theor. Phys. **97**, 875 (2003)].
[13] A. V. Taichenachev, A. M. Tumaikin, V. I. Yudin, and G. Nienhuis, Phys. Rev. A **69**, 033410 (2004).
[14] We use the standard definiton for the saturation intensity, see, e.g., in C. S. Adams and E. Riis, Prog. Quantum Electron. **21**, 1 (1997).
[15] O. N. Prudnikov, A. V. Taichenachev, A. M. Tumaikin, and V. I. Yudin, Zh. Eksp. Teor. Fiz. **120**, 76 (2001) [J. Exp. Theor. Phys. **93**, 63 (2001)].
[16] A. V. Bezverbny, G. Nienhuis, and A. M. Tumaikin, Opt. Commun. **148**, 151 (1998).
[17] J. Javanainen, Phys. Rev. A **46** 5819 (1992).
[18] G. Grynberg and C. Robilliard, Phys. Rep. **355**, 335 (2001).
[19] Th. Schulze, T. Müther, D. Jürgens, B. Brezger, M. K. Oberthaler, T. Pfau, and J. Mlynek, Appl. Phys. Lett. **78**, 1781 (2001).